Device Modeling of Statistical Dopant Fluctuations in MOS Transistors

P.A. Stolk, F.P. Widdershoven, and D.B.M. Klaassen
Philips Research Laboratories
Prof. Holstlaan 4, 5656 AA Eindhoven, The Netherlands
Tel: +31-40-2743670. E-mail: stolk@natlab.research.philips.com

Abstract -- This paper addresses the numerical requirements for device modeling of statistical dopant fluctuations in MOS transistors. It is found that the standard deviation of the threshold voltage V_T can be properly derived from 2D or 3D simulations using a relatively coarse simulation grid. Evaluating the threshold voltage shift arising from dopant fluctuations, on the other hand, calls for a full 3D approach with a numerical grid that is sufficiently refined to represent the discrete nature of the dopant distribution. The average V_T-shift is found to be positive for long, narrow devices, and negative for short, wide devices.

I. INTRODUCTION

Experiments and device simulations [1-6] have shown that the standard deviation σ_{V_T} in the threshold voltage V_T of submicron MOSFETs is determined to a large extent by statistical dopant fluctuations in the channel depletion region. Device simulations have indicated that dopant variations also yield a shift in the average threshold voltage $<V_T>$ compared to V_T calculated for unperturbed doping profiles. Both negative and positive V_T-shifts have been reported [3,4,6], but no consensus has been reached as to the origin of these V_T-shifts. Moreover, no extensive analysis has been reported until now of how numerical procedures affect the calculated results for σ_{V_T} and $<V_T>$. In order to address these issues, 2D and 3D MINIMOS simulations are used to identify the dependence of σ_{V_T} and $<V_T>$ on transistor design and geometry, the numerical gridding procedure, and the dimensionality of the device simulations.

II. METHOD

In order to introduce statistical dopant fluctuations into the numerical calculations, the simulated devices are subdivided into cells with sizes ΔX_C, ΔY_C, and ΔZ_C in the direction of the length (L), depth, and width (W) of the device, respectively. For each cell its actual number of dopants $\tilde{n}$ is drawn independently from a Poisson distribution with expectation value $n=N\Delta X_C\Delta Y_C\Delta Z_C$, where N is the dopant concentration used in the conventional, unperturbed simulations. To introduce fluctuations, N in each cell is replaced by $\tilde{N}=\tilde{n}/(\Delta X_C\Delta Y_C\Delta Z_C)$. In the case of 2D simulations, $\Delta Z_C=W$ is used.

The cell sizes used in the present simulations typically yield values for n in the range from ~1 to 10. Unrealistic simulation results are obtained when applying minute cell volumes with expectation values of $n\ll 1$. In that case, the randomized doping distribution comprises a few cells with $\tilde{N}\gg N$ amidst a multitude of cells with $\tilde{N}=0$. Apparently, such a highly discrete representation of the dopant distribution precludes stable numerical modeling when using a continuum device simulator.

In this study, simulations are performed for NMOS transistors with an acceptor concentration N_A of 10^{18} cm^{-3} and a gate-oxide thickness T_{ox} of 4 nm. The electron mobility is taken constant at 350 cm^{2}V^{-1}s^{-1}. The threshold voltage V_T is calculated at a drain bias of 0.1 V using a current criterion of (100 nA)×W/L. The statistical distribution of V_T is obtained by simulating the same device structure several times, each time with a newly generated random dopant distribution.

III. RESULTS AND DISCUSSION

A. 2D Simulations

In order to check the numerical grid spacing that is required for modeling the randomized device structures, the following 2D simulations are performed. For a fixed choice of ΔX_C=15 nm and ΔY_C=3 nm, the numerical grid spacings ΔX_{GR} and ΔY_{GR} are varied. Figures 1 and 2 summarize the calculated standard deviation and

0-7803-3775-1/97/$10.00 © 1997 IEEE.

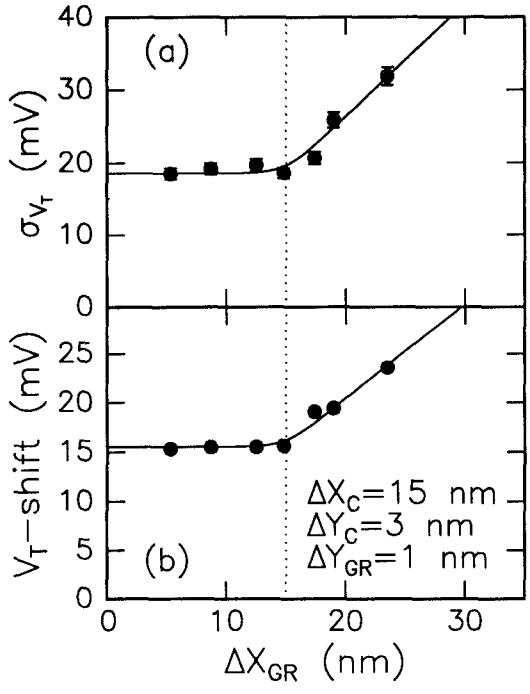

Figure 1. *2D MINIMOS simulations of (a) the standard deviation and (b) the average value of the threshold voltage V_T as a function of the numerical grid size ΔX_{GR} (L=0.4 μm, W=0.05 μm). The vertical grid size is taken as ΔY_{GR}=1 nm. The cell sizes used to define the dopant fluctuations are fixed at ΔX_C=15 nm and ΔY_C=3 nm. The average V_T-value is plotted as the shift with respect to V_T calculated for an unperturbed dopant distribution. Each point was derived from 300 statistical simulations. The solid lines serve to guide the eye.*

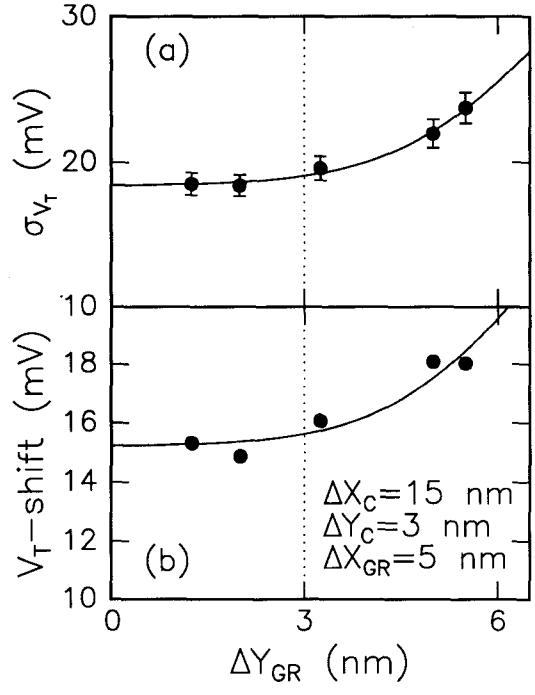

Figure 2. *Same as Fig. 1, but now with ΔX_{GR} fixed at 5 nm and ΔY_{GR} varying.*

average value of V_T as a function of ΔX_{GR} and ΔY_{GR}, respectively. When using $\Delta X_{GR}>\Delta X_C$ (Fig. 1) or $\Delta Y_{GR}>\Delta Y_C$ (Fig. 2), both σ_{V_T} and $<V_T>$ increase with increasing grid spacings because the numerical grid becomes too coarse to properly deal with the variations in the dopant concentration imposed by ΔX_C and ΔY_C. On the other hand, the values for σ_{V_T} and $<V_T>$ are independent of the numerical grid size as long as $\Delta X_{GR}\leq\Delta X_C$ (Fig. 1) and $\Delta Y_{GR}\leq\Delta Y_C$ (Fig. 2). Similar conclusions are obtained for other choices of ΔX_C and ΔY_C. Therefore, this numerical test implies that dopant fluctuations can be modeled by choosing ΔX_C and ΔY_C directly on the basis of the numerical grid (i.e., $\Delta X_C=\Delta X_{GR}$; $\Delta Y_C=\Delta Y_{GR}$) without affecting numerical consistency. In fact, this approach will be used from here on to define statistical variations in both the acceptor and donor distributions. In the case of 3D simulations, ΔZ_C is taken equal to the numerical grid size ΔZ_{GR} along the channel width.

After having established the requirements on the numerical grid, we continue to investigate the appropriate choices for ΔX_C and ΔY_C for modeling dopant fluctuations. Figure 3 shows σ_{V_T} and $<V_T>$ derived from 2D simulations using various values for ΔX_C. The calculated standard deviation in V_T does not change with varying ΔX_C. In fact, σ_{V_T} is independent of the cell size as long as the channel depletion region is subdivided into a sufficient number of cells into the depth direction (roughly more than 5 in case of a uniform doping profile). Since surface potential and field fluctuations are determined by a *linear* superposition of the individual contributions of isolated ionized impurities, calculating the effect of charge variations on σ_{V_T} should indeed be independent of the device area over which these variations are averaged, as observed. Additional simulations [see also Ref. 5] show that σ_{V_T} scales linearly with T_{ox}, $N_A^{1/4}$, and $(W\times L)^{-1/2}$, which is qualitatively consistent with experimental results [1] and with an analytical expression which describes σ_{V_T} in terms of the overall dopant number variation inside the

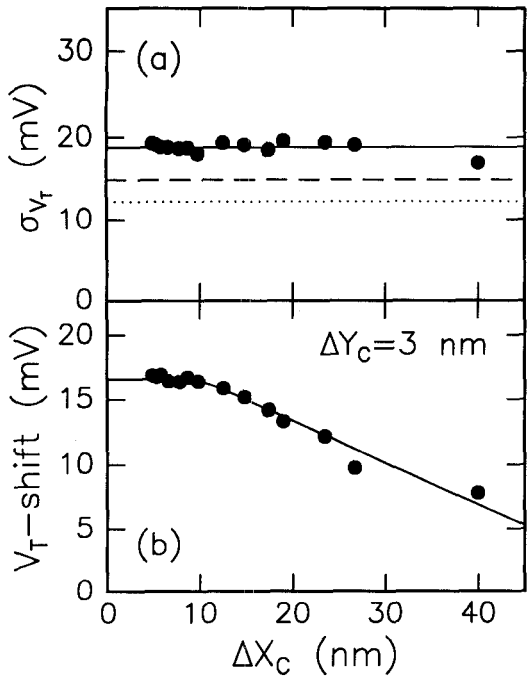

Figure 3. *2D MINIMOS simulations of (a) σ_{V_T}; (b) V_T-shift as a function of the cell size ΔX_C (L=0.4 μm, W=0.05 μm). The vertical cell size ΔY_C in the depletion region is ~3 nm, with a further refinement of ~1 nm inside the channel inversion layer. Each point was derived from 900 statistical simulations. The solid lines serve to guide the eye. The dotted and dashed lines in (a) represent analytical expressions for σ_{V_T} from [5] and [7], respectively (see text).*

channel depletion region [5]. Improved quantitative agreement [Fig. 3(a)] is obtained using a modified analytical expression, which explicitly takes the depth-distribution of depletion charges into account [7].

In contrast to the behavior of σ_{V_T}, the calculated V_T-shift is found to increase upon decreasing ΔX_C, leveling off at ~17 mV for $\Delta X_C \leq 12$ nm. This indicates that modeling of $\langle V_T \rangle$ requires the cell spacing along the channel to be sufficiently dense (i.e., $\Delta X_C \leq 12$ nm) in order to properly represent the discrete nature of the dopant fluctuations and the corresponding variations in the surface potential. As demonstrated by the simulations in Fig. 4, this cell dimension is physically realistic in that it captures the typical range over which the surface electron concentration is disturbed upon adding one acceptor to the depletion layer. It is expected that a similar constraint applies to ΔZ_C along the channel width in the case of 3D simulations. Finally, the results for σ_{V_T} and

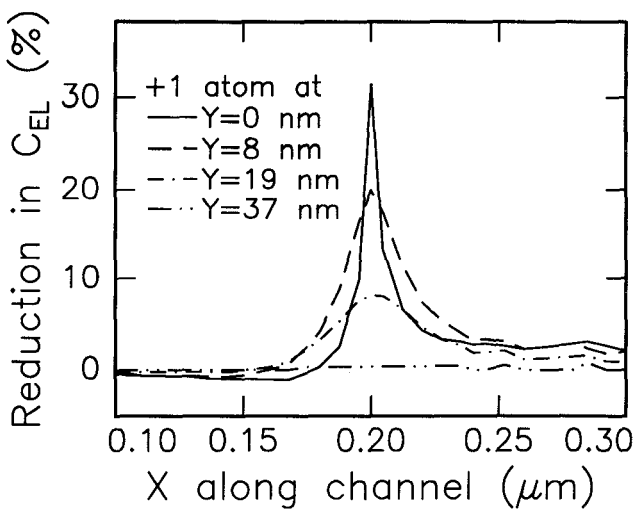

Figure 4. *2D simulations of the reduction in surface electron concentration C_{EL} in response to adding one acceptor to an otherwise uniform channel dopant distribution (i.e., no fluctuations applied). The device dimensions are as in Fig. 3. The gate is biased at the threshold voltage, the drain at 0.1 V. The extra acceptor atom is positioned at X=L/2 and at various depths, as indicated.*

$\langle V_T \rangle$ are found to be almost independent of the value taken for ΔY_C as long as $\Delta Y_C < 10$ nm, with the additional inclusion of ~1 nm spacings inside the near-surface inversion layer.

B. Comparing 2D and 3D Simulations

Figure 5 shows a comparison of 2D and 3D simulations for transistors with various length-to-width ratios. The active device area is kept constant at $W_{eff} \times L_{eff} = 0.024$ μm^2 in order to ensure the same overall dopant variation for all geometries. Indeed, the calculated standard deviation in V_T in Fig. 5(a) is ~17 mV regardless of the device geometry or simulation dimensionality. Only for very small channel lengths ($L_{eff} < 0.04$ μm) does σ_{V_T} increase as a result of charge sharing in the source and drain depletion regions [1,5]. No significant V_T-shift is observed in 2D simulations for gate lengths smaller that 0.1 μm, in contrast to the negative V_T-shifts reported for 2D simulations in Ref. [3]. This discrepancy could originate from, for instance, different vertical cell spacings used inside the channel inversion layer, or from differences in expectation value *n*, but further studies are needed to resolve this issue.

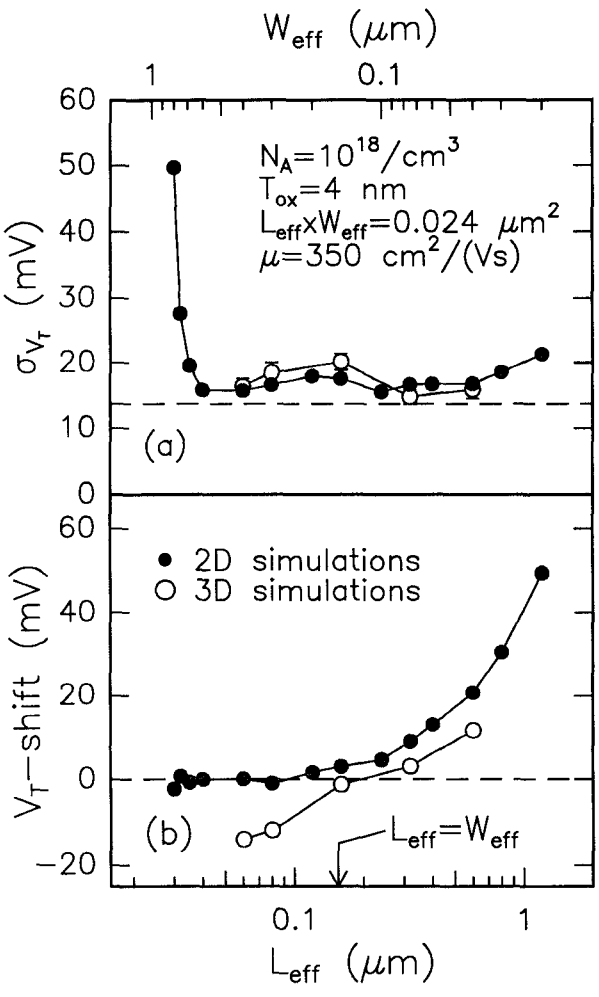

Figure 5. *Calculated σ_{V_T} and V_T-shift using 2D and 3D simulations with $\Delta X_C<15$ nm, $\Delta Z_C<15$ nm, and $\Delta Y_C< 7$ nm. The active device area is kept constant while varying W_{eff}/L_{eff}. The dashed line in (a) represents an analytical expression for σ_{V_T} [7].*

For $L_{eff}>0.1$ µm, the V_T-shift in 2D simulations progressively increases with increasing gate lengths. This trend reflects the enhanced probability that the statistically modified dopant distribution comprises a "high-doping" region along the channel as the gate length is increased, resulting in a positive shift of $<V_T>$. In 3D simulations, the calculated V_T-shift changes sign from positive for $L_{eff}>W_{eff}$ to negative for $L_{eff}<W_{eff}$. The positive V_T-shift for long devices is less pronounced than in 2D simulations because of the relaxed constraints on current paths in three dimensions. The negative V_T-shift for short devices reflects the enhanced probability of having a conductive "short" from source to drain when the device length is reduced. This percolation behavior [8] is only properly modeled with a full-blown 3D approach.

IV. CONCLUSIONS

This study comprises a detailed analysis of the numerical procedures for modeling statistical dopant fluctuations in MOS transistors. The calculated standard deviation in V_T is only weakly dependent on the numerical cell sizes through which the dopant fluctuations are introduced into the simulation grid. This implies that σ_{V_T} can be properly estimated by means of 2D or 3D simulations with a relatively coarse representation of the dopant fluctuations. Correct modeling of the average value of V_T, on the other hand, requires a careful analysis of the appropriate cell size for the device under investigation (i.e., $\Delta X_C \leq 12$ nm for $N_A=10^{18}/cm^3$ and $T_{ox}=4$ nm). The direct comparison between 2D and 3D simulations reveals that evaluating the dependence of $<V_T>$ on transistor geometry calls for a 3D approach in order to include the effects of three-dimensional current paths.

REFERENCES

[1] T. Mizuno et al., IEEE Trans. Electron Dev. vol. 41, 2216 (1994).

[2] M. Eisele, J. Berthold, R. Thewes, E. Wohlrab, D. Schmitt-Landsiedel, and W. Weber, Tech. Dig. IEDM-95, 67 (1995).

[3] K. Nishinohara, N. Shigyo, and T. Wada, IEEE Trans. Electron Dev. vol. 39, 634 (1992).

[4] H.-S. Wong and Y. Taur, Tech. Dig. IEDM-93, 705 (1993).

[5] P. A. Stolk and D. B. M. Klaassen, Tech. Dig. IEDM-96, 627 (1996).

[6] V. K. De, X. Tang, and J. D. Meindl, Tech. Dig. VLSI Techn. Symp., 198 (1996).

[7] F.P. Widdershoven, unpublished.

[8] R.W. Keyes, Appl. Phys. vol. 8, 251 (1975).